J Mater Sci (2007) 42:510–521
DOI 10.1007/s10853-006-1259-1

Microstructural development and solidification cracking susceptibility of Cu deposits on steel: Part II—use of a Ni interlayer

Fredrick F. Noecker II · John N. DuPont

Received: 17 June 2004 / Accepted: 13 January 2006 / Published online: 28 December 2006

Abstract The tool and die industry is interested in depositing Cu onto steel using direct metal deposition techniques in order to improve thermal management of mold dies manufactured from steel alloys. However, Cu is a known promoter of solidification cracking in steel. Ni, however, is known to improve weldability of Cu containing alloys and steel. The goal of this work was to identify the range of Ni concentrations necessary to eliminate solidification cracking in Steel–Cu deposits and understand the cracking susceptibility through analysis and modeling of microstructural development. A wide range of Steel–Ni–Cu deposits, containing up to 75 wt% Ni, and Ni–Cu deposits were fabricated using the Gas Tungsten Arc Welding (GTAW) process with cold wire feed. The Ni–Cu and Fe–Ni deposits were found to be crack free over the entire concentration range. However, Ni concentrations of up to 75 wt% were insufficient to eliminate cracking when subsequent layers of Cu were deposited. Therefore, to ensure crack free deposition of Cu onto Steel, the concentration of the interlayer must be 100 wt% Ni. The resultant microstructures were characterized by various microscopy techniques to understand the influence of Ni and Cu on solidification cracking of Steel. Additionally, solidification modeling was undertaken to determine the amount of terminal Cu rich liquid and solidification temperature range that would form under non-equilibrium solidification conditions.

F. F. Noecker II (✉) · J. N. DuPont
Engineering Metallurgy Group, Department of Materials Science and Engineering, Lehigh University, Bethlehem, PA, USA
e-mail: ffn2us@yahoo.com

Introduction

Direct metal deposition (DMD) processes, like Laser Engineered Net Shaping™ (LENS™) offer the unique advantages of producing fully dense three-dimensional metallic parts directly from a computer aided design drawing. As such, the tool and die industry would like to harness the advantages of direct metal deposition processes to fabricate molds with functionally graded compositions in order to improve mold performance. One possible means to improve the thermal conductivity of tool steel molds is to selectively deposit Cu using a compositional gradient. The thermal conductivity of Cu is nearly 13 times greater than H-13 tool steel [1, 2], and its use in this application would translate into shorter mold cycle times and increased mold productivity.

However, copper has been shown by several researchers to promote solidification cracking/hot cracking in steel [3–6]. Attempts to deposit Cu onto tool steel using a direct metal depositions process have also been hampered by solidification cracking [7]. Additional work that used AISI 1013 Steel and Cu as a model system examined the effects of Cu concentration on solidification cracking. Solidification cracks were found to form in deposits with Cu concentration between 5 wt% and 43 wt% [8]. One potential solution is to avoiding solidification cracking when depositing Cu onto steel is to carefully control the dilution‘ to ensure the fusion zone Cu concentration does not drop below 50 wt%. However, in cases where dilution cannot be accurately controlled, or design considerations require a copper concentration within the crack susceptible region, an alternative approach is required.

Two primary metallurgical controlling factors in solidification cracking are the solidification temperature range and the amount of terminal liquid at the end of solidification. Nickel has been shown to increase the solubility of Cu in austenite [9], which should result in a concomitant reduction of the amount of terminal Cu rich liquid and solidification cracking susceptibility. Several researchers have found that the addition of Ni, either as an interlayer or as an alloying element with Cu, decreases the cracking susceptibility when Cu is deposited on Steel [10–12]. The addition of Ni is also expected to improve the thermal conductivity of the molds, due to its thermal conductivity being more than twice that of H-13 [1].

The equilibrium phase diagrams for Fe–Ni and Cu–Ni are given in Fig. 1 [13]. The Fe–Ni phase diagram exhibits a very small solidification temperature range. Additionally, it is nearly isomorphous, with almost complete solid solubility at elevated temperatures, and would therefore be expected to contain no terminal liquid at the end of solidification. The Cu–Ni system is isomorphous, but does have a larger solidification temperature range than the Fe–Ni system for both equilibrium and non-equilibrium Scheil [14] solidification

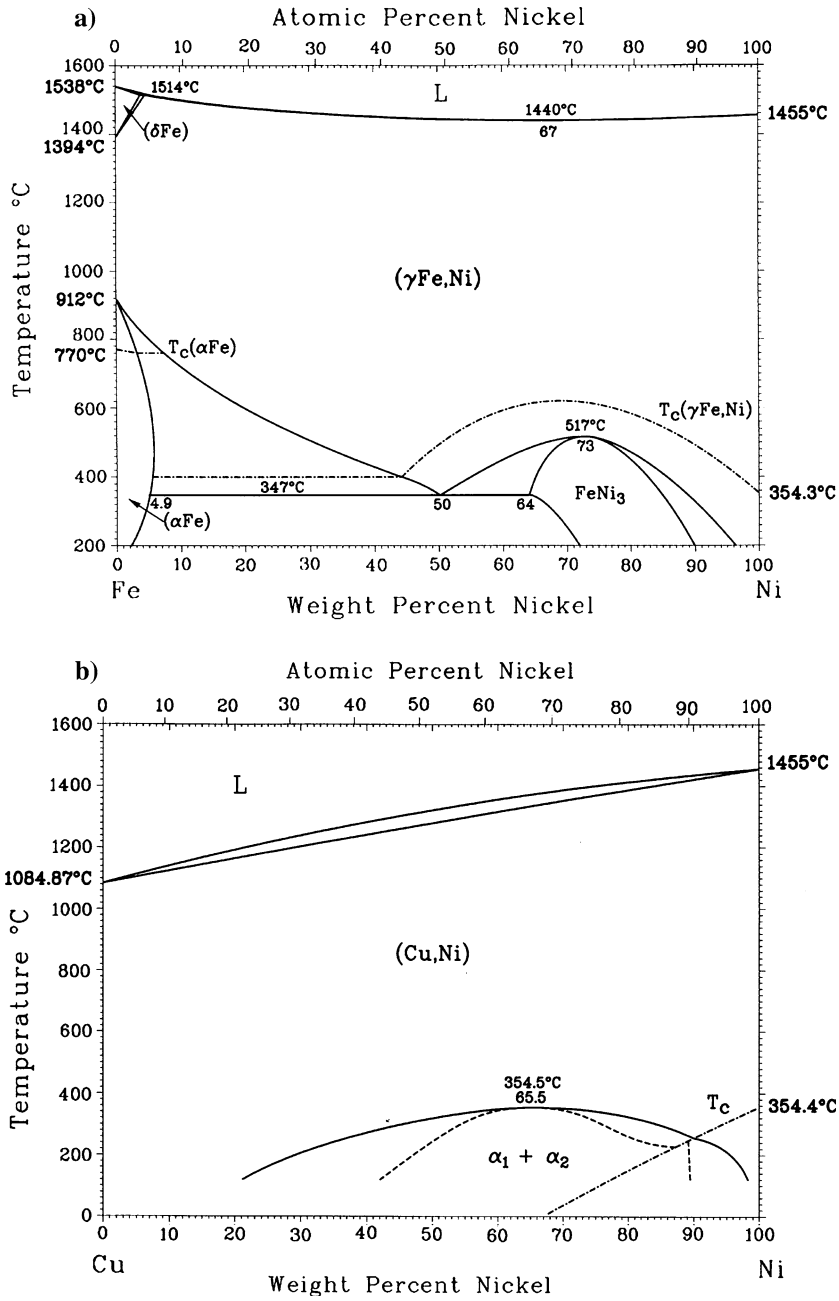

Fig. 1 Phase diagrams [13] for (**a**) Fe–Ni and (**b**) Cu–Ni

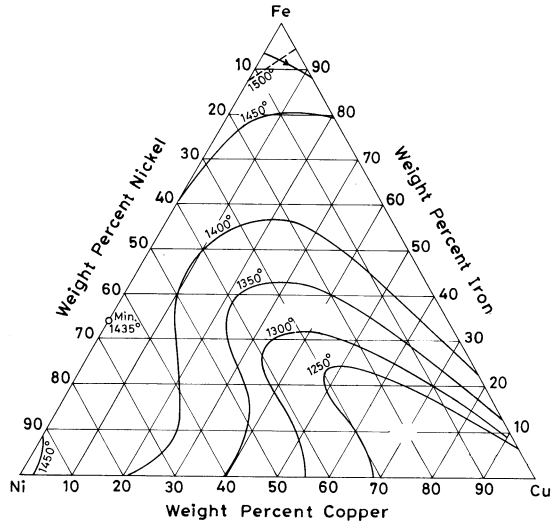

Fig. 2 Fe–Ni–Cu liquidus projection [15]

conditions. Scheil conditions are defined as equilibrium at the solid/liquid interface, no undercooling, infinite diffusion in the liquid and negligible diffusion of solute in the solidifying solid. Because both binary systems are almost completely isomorphous, they are expected to have low solidification cracking susceptibility.

According to the Fe–Ni–Cu liquidus projection, the minimum temperature occurs in the pure Cu phase at 1085 °C (Fig. 2 [15]). Under Scheil conditions the composition of the terminal liquid is expected to be enriched to a minimum in the system. As such, Cu is expected to be the terminal point in the ternary system if Scheil solidification conditions exist, thereby resulting in an enlarged solidification temperature range as compared to equilibrium solidification conditions.

The objective of this work is to determine the minimum Ni interlayer concentration necessary to produce crack free Fe–Ni–Cu compositionally graded deposits. In this study, Ni–Cu and Fe–Ni–Cu weld deposits were made using the Gas Tungsten Arc Weld (GTAW) process and examined for cracking. Cracking susceptibility of Fe–Ni–Cu deposits was quantified through microstructural analysis and explained through solidification modeling. The results of this work will provide insight towards the development of a deposition process that can combine Cu and tool steel for the die industry and the manufacturing community as a whole.

Experimental procedure

To represent the Fe–Ni–Cu ternary system, SAE 1013 Steel (bar), Ni 99 (wire), Ni 200 (bar) and deoxidized (DEOX) Cu (wire) were chosen as base and filler metal materials. This model system will simplify the analysis by reducing the number of trace alloying elements, while producing results representative of the solidification behavior of tool steel, Ni and Cu. The compositions for the alloys used in this work are listed in Table 1.

The current work only considers compositional effects on solidification cracking. Therefore, a Gas Tungsten Arc Weld (GTAW) system with a cold wire feed was used to produce bead on plate deposits as described elsewhere [8]. A wide range of binary Ni–Cu compositions were fabricated by depositing a single pass bead-on-plate deposit. DEOX Cu (1.143 mm diameter) filler metal wire was deposited onto rolled Ni 200 plate that was 0.635 cm thick and cut to 2.54 cm width.

To produce Fe–Ni–Cu deposits, multiple bead-on-plate deposits were prepared one on top of the other to simulate the direct metal deposition process. The first layer consisted of Ni-99 (1.143 mm diameter) filler metal wire deposited onto SAE 1013 steel. A second pass of Ni-99 was required to produce deposits with over 60 wt% Ni, and was deposited on top of the first

Table 1 Material compositions in wt%

	C	Mn	Si	S	P	Cr	Ni	Mo	Cu	Fe	Al	Sn	Ti
Cu wire	–	0.18	0.23	–	0.01	–	–	–	98.78	–	–	0.8	–
Ni 99 wire	0.03	–	0.12	0.001	0.004	–	99.8	–	–	0.053	0.001	–	0.002
SAE 1013 bar	0.13	0.82	0.173	0.02	0.007	0.026	0.066	0.015	0.08	98.643	0.009	0.011	–
Ni 200 bar	0.04	0.18	0.03	0.001	–	–	99.7	–	0.01	0.05	–	–	–

Table 2 GTAW processing parameters

Material	Arc gap (mm)	Travel speed (mm/s)	Arc potential (volts)	Arc current (amperes)	Wire feed speed (mm/s)
Cu onto Ni99	2.54	2	10	325–130	8–45
Ni onto 1013	2.54	2	10	375–325	4–71
Cu onto Fe–Ni	2.54	2	10	200–125	4–25

bead of Ni. Subsequent layers of Cu were deposited on top of the Fe–Ni layer by using DEOX Cu. The composition of each pass was varied by changing the filler metal feed rate and the arc current. The GTAW processing parameters for each condition are given in Table 2. The shielding gas was commercially pure Ar.

The welds were visually examined for surface cracks after each weld pass. The nature of the cracks was determined by examining a transverse cross-section from each multi-pass build-up. For example, the build-up in Fig. 3a would be one metallographic sample used to examine the microstructure (including cracking where applicable) in all five layers. In all cases there was a direct correspondence between observed surface cracks and cracking in the transverse cross-sections. Stated another way, all cracks that formed did so upon initial solidification and not due to reheat.

Transverse cross-sections of samples from each processing condition were prepared using standard metallographic techniques. Cu rich regions were revealed by etching with equal parts 30% hydrogen peroxide, concentrated ammonia and distilled water. The Fe–Ni samples were pre-etched in 30% nirtric/70% methanol followed by etching in a 35% aqueous solution of sodium metabisulfite to reveal cell boundaries.

Both bulk and point compositions were determined with an electron-probe microanalyzer (EPMA). A JEOL 733 Super Probe, equipped with wavelength dispersive spectrometers (WDS), was operated at an accelerating voltage of 20 kV and a probe current of 25 nA for bulk analysis. To minimize the excitation volume yet maintain sufficient over voltage to generate Cu K_α X-rays, the accelerating voltage was reduced to 15 kV for point analysis. To measure the nominal composition of the deposits, three to six measurements were acquired on each deposit from an area approximately 2000 μm^2 per measurement. This area was

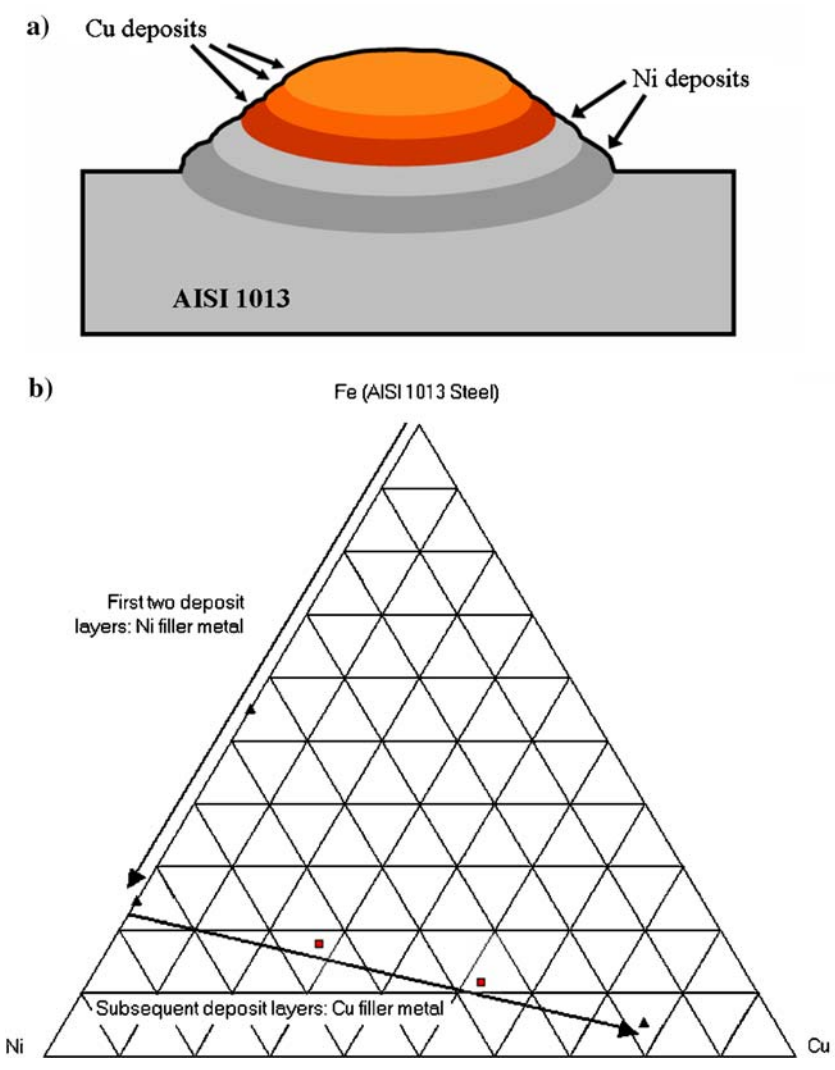

Fig. 3 (**a**) Schematic of multi pass Fe–Ni–Cu deposits and (**b**) resultant compositions of each layer plotted on Fe–Ni–Cu ternary diagram. Triangles represent compositions that did not crack and squares represent compositions that did crack

large enough to average out variations in composition due to microsegregation and provide good statistical measurement of the nominal deposit composition. A phi(ρZ) correction method was utilized to convert X-ray counts to weight percentages [16]. Compositional data was normalized for weight percent Fe, Ni and Cu, which is reasonable given the maximum amount of trace elements present in any deposit is 1.36 wt%, according to wet chemical analysis of the raw material.

Quantitative image analysis (QIA) was used to perform area fraction measurements of the Cu rich phase, which were assumed equivalent to the volume fraction. Twenty fields of view were measured for each composition to provide good statistical confidence in the area fraction measurements.

Results

Figure 3 is a schematic of a transverse cross-section of one such multi layer deposit with an example of accompanying compositions of each layer plotted on the Fe–Ni–Cu ternary phase diagram. Ni filler metal is deposited on AISI 1013 Steel for the first two layers, which moves the composition of each deposit towards the Ni rich corner of the ternary. Subsequent layers were fabricated by using Cu filler metal wire, thereby increasing the Cu content of each layer and moving the composition towards the Cu rich corner. Figure 4 is a summary of the solidification cracking results for the Fe–Ni–Cu deposits with results for the Fe–Cu system included from Part I [8]. Solidification cracking was not observed in the binary Fe–Ni and Ni–Cu deposits, however, solidification cracks were observed in nearly all the ternary Fe–Ni–Cu deposits even with an interlayer consisting of up to 75 wt% nickel.

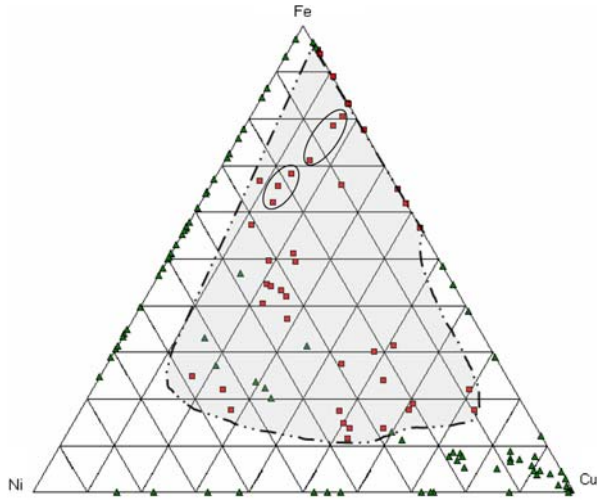

Fig. 4 Solidification cracking results. Squares and triangles represent cracked and crack free compositions, respectively. Dotted line defines crack susceptible composition range. Volume percent Cu rich phase for encircled data points displayed in Fig. 7

A comparison of Figs. 5 and 6, light optical micrographs of Fe–2.5Ni–17.0Cu and Fe–13.2Ni–15.5Cu samples, respectively, provide insight into the cracking mechanism. Cracking is observed exclusively along Cu cell and grain boundaries, which are the last solid to form. Additionally increasing the Ni content with similar nominal Cu concentration results in the formation of less terminal Cu during solidification. The effects of Ni additions on the amount of terminal Cu rich phase for approximately constant nominal Cu concentrations (16.4 ± 0.7 wt% Cu and 13.3 ± 0.5 wt% Cu) is presented in Fig. 7. The volume percent of Cu rich phase in Fe–Ni–Cu deposits with similar Cu concentration but changing Fe to Ni ratio are plotted. As expected, exchanging Ni for Fe reduces the amount of terminal Cu due to the increased solubility of Cu [9]. Conversely, an increase in Cu concentration with similar Fe–Ni ratio is expected to result in a greater amount of Cu rich phase. This can be seen in the light optical micrograph for the Fe–10.0Ni–24.0Cu deposit (Fig. 8), which has 12.8 vol% Cu phase, as compared to Fig. 6, which has a similar Fe–Ni ratio, but a lower Cu concentration and only 4.7 vol% Cu.

When both Ni and Cu concentrations are increased the microstructure changes from two phase to single phase as seen for the Fe–28.2Ni–57.8Cu alloy in Fig. 9. Cracking, along with some porosity (black spots), is observed along the Cu rich regions, however, these Cu rich regions do not appear to form a distinct second phase. Additionally, no liquid films were observed adjacent to the cracks thereby ruling out the presence of low melting point impurities. Figure 9 is representative of the second class of ternary microstructure and

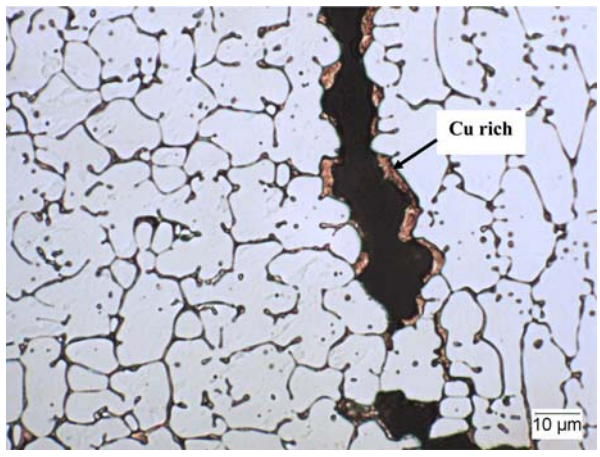

Fig. 5 Light optical micrograph of etched Fe–2.5Ni–17.0Cu deposit. Cracking observed along Cu rich regions

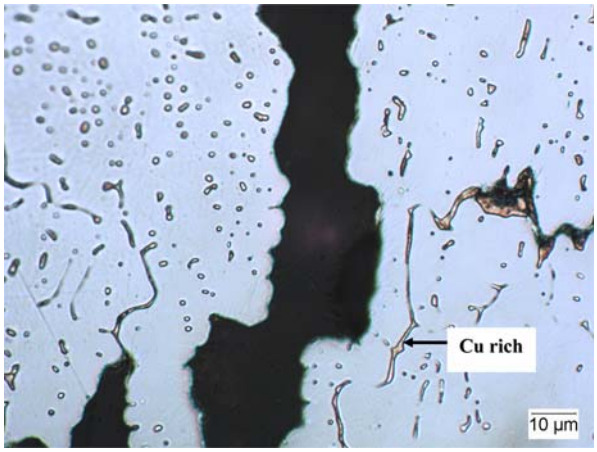

Fig. 6 Light optical micrograph of etched Fe–13.2Ni–15.5Cu. Cracking along Cu rich regions. Increased Ni results in less terminal Cu compared to Fig. 5

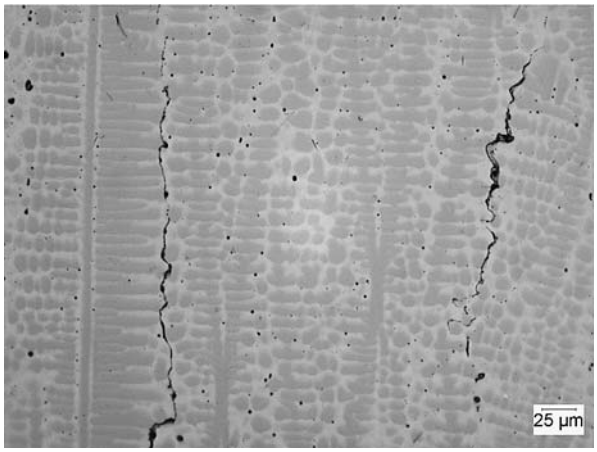

Fig. 9 Light optical micrograph of as-polished Fe–28.2Ni–57.8Cu deposit. Change in morphology compared to lower Ni deposits, however, cracking is still observed along Cu rich regions

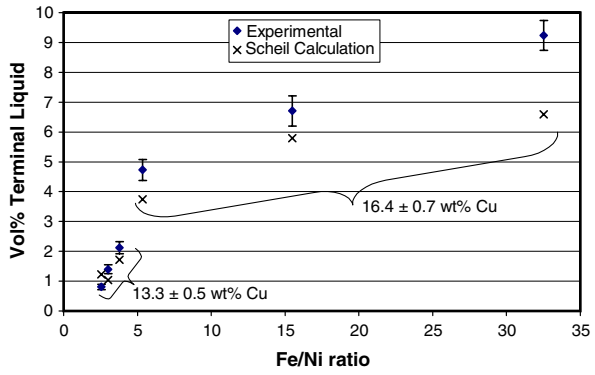

Fig. 7 Effect of Ni concentration on Cu rich phase in Fe–Ni–Cu alloys

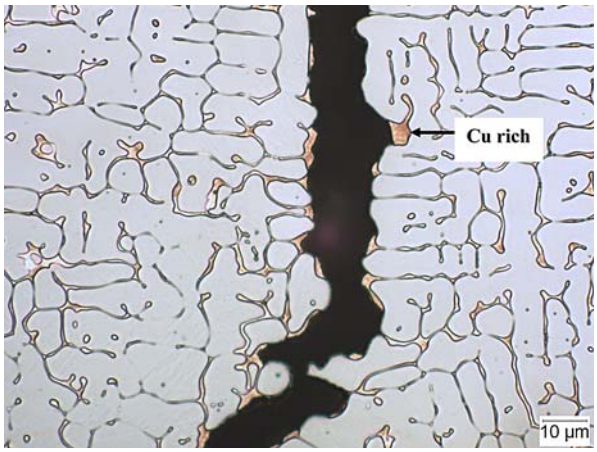

Fig. 8 Light optical micrograph of etched Fe–10.0Ni–24Cu deposit exhibiting cracking along Cu rich phase. Increased amount of Cu rich phase as compared to Fig. 6, which has similar Ni content but less Cu

alludes to a change in solidification behavior, which will be discussed in the next section.

Discussion

Solidification behavior

As has been shown for the Fe–Cu system [8] solidification behavior and the nominal composition control the solidification temperature range and amount of terminal liquid. Two key metallurgical factors to solidification cracking susceptibility are the solidification temperature range and amount of terminal liquid. To understand cracking susceptibility it is necessary to determine the solidification behavior, which is a function of the dimensionless back diffusion parameter, α [17]. Solidification behavior is bounded by equilibrium and non-equilibrium (Scheil) conditions. The upper and lower bounds for the amount of terminal liquid and the solidification temperature range can be determined by these two solidification conditions.

It has been shown that microsegregation in welds is a function of the back diffusion potential of solute elements in the solidifying solid as the weld freezes [17–21]. Assuming a constant portioning coefficient, alloy systems with a small back diffusion potential will experience greater levels of microsegregation during solidification. The greater microsegregation will produce a larger amount of terminal solute rich liquid, which will impact the solidification cracking susceptibility of the alloys system.

To determine the solidification behavior of Fe–Ni–Cu alloys, and the amount of terminal Cu rich liquid that would form during solidification, the dimensionless back diffusion coefficient α must be calculated. Once the solidification behavior is known, the solidification temperature range and amount of terminal liquid can be determined.

In order to determine the solidification condition for the Fe–Ni–Cu ternary system, the dimensionless back diffusion parameter (α) was calculated for the three binary systems. If all three binary systems have negligible back diffusion potential, then it is reasonable to assume that the back diffusion potential for compositions within the Fe–Ni–Cu system is negligible as well. A detailed calculation of the back diffusion parameter can be found in a previous work [8]. The essential elements of its calculation for the Fe–Ni–Cu system are given below.

The back diffusion potential for the Fe–Cu system was found to be negligible when the primary solidification phase was either δ or γ ($\alpha = 0.0054$ and 0.0007, respectively) [8]. The back diffusion potential for the Fe–Ni and Ni–Cu samples were determined using Fe–24.0Ni and Ni–15.5Cu samples, respectively. Following the Brody and Fleming [17] solidification model, α is a function of D_s, the diffusivity of the solute (Ni or Cu) in the solid (γ Fe or Ni), t_f, the solidification time, and L, the distance the solute must travel to eliminate any compositional gradient, which is half the dendrite arm width.

The solidification time, t_f, is determined by the ratio of the solidification temperature range, ΔT and the cooling rate, assuming that the cooling rate is linear within the solidification temperature range. The Rosenthal equation for three-dimensional heat flow from a point heat source was used to estimate the cooling rate along the weld center line [22]. The thermal conductivity, λ, for Fe and Ni at 727 °C is 0.326 and 0.718 W/(cm °C), respectively [1]. These values were used as the effective thermal conductivity. The conditions used to make the deposits were, VI = 3,250 W, S = 0.2 cm/s, $\eta_a = 0.75$ for the GTAW process [23], T_o = 25 °C, and T = 1465 and 1428 °C (liquidus temperature) for Fe–Ni and Ni–Cu, respectively. Given the above, the Rosenthal approximated cooling rate was found to be 349 °C/s for Fe–Ni and 729 °C/s for Ni–Cu. The maximum solidification temperature range for Fe–Ni and Ni–Cu was 25 °C and 343 °C, respectively. The resultant solidification time was 0.07 s and 0.5 s for Fe–Ni and Ni–Cu, respectively.

Because diffusivity is dependant on temperature, the value of the back diffusion potential will change as the deposit cools. Therefore, an upper bound estimation is made for the back diffusion potential (α_{max}) of both Fe–Ni and Ni–Cu samples. If α_{max} is found to be $\ll 1$, then both alloys will solidify under non-equilibrium conditions regardless of temperature.

To provide an upper bound estimation for α, the diffusivities of Ni in γ Fe and Cu in Ni were calculated at the respective liquidus temperatures. Diffusivity of Ni in γ Fe at 1465 °C and Cu in Ni at 1428 °C was found to be 1.1×10^{-13} m^2/s and 1.23×10^{-12} m^2/s, respectively [24]. The dendrite arm spacing was measured to be 20.7 and 11.3 μm for Fe–Ni and Ni–Cu, respectively. The resultant α_{max} for Fe–Ni and Ni–Cu is then 0.00007 and 0.02, both of which are $\ll 1$. Since $\alpha_{max} \ll 1$ for the three constitutive binary systems, the solidification conditions for ternary Fe–Ni–Cu alloys are expected to be close to non-equilibrium Scheil conditions.

Solidification modeling

The solidification temperature range and amount of terminal liquid are two key metallurgical factors in the solidification cracking susceptibility of an alloy. The advent of computational thermodynamic programs, such as ThermoCalc [25–27], enables the calculation of these two parameters over a broad range of Fe–Ni–Cu compositions. The use of the Scheil module [28] provides a means for predicting these values even when the equilibrium partition coefficient (k) varies with temperature and composition. It is anticipated that k will vary in Fe–Ni–Cu ternary space given that it is not constant with varying temperature and compositions for the three associated binary diagrams.

Figure 10 displays the results of solidification calculations performed by ThermoCalc for the Fe–Ni–Cu system. Composition was varied by 10 wt% per calculation. The solidification temperature range and weight fraction of terminal liquid, in parenthesis, were calculated for the Scheil solidification condition. It was possible to carry out these calculations over the majority of the Fe–Ni–Cu system, except towards the Cu rich region. Scheil data from previous work [8] was used to complete the Fe–Cu binary results. It was not possible to perform a ThermoCalc Scheil calculation on compositions in the Cu rich corner. For this reason, the solidification temperature range and amount of terminal liquid is listed with question marks for the Fe–10Ni–80Cu composition. The boundary from Fig. 4 which approximately separates crack susceptible and crack free deposits is superimposed in Fig. 10. From these results two observations can be made. First, a large solidification temperature range of over 150 °C is present for nearly all ternary compositions with solidi-

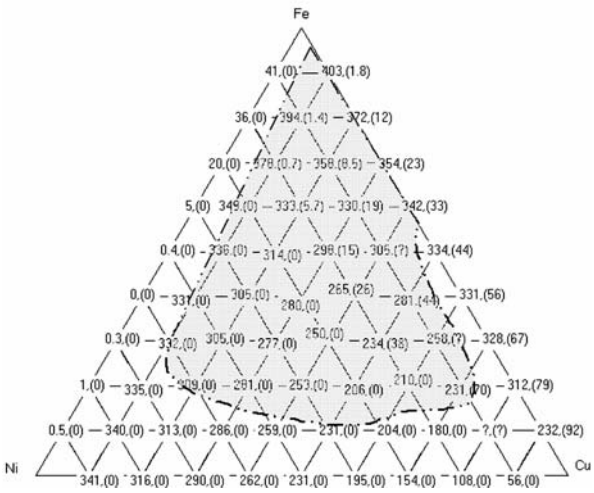

Fig. 10 Solidification temperature range in °C and volume percent terminal Cu (in parenthesis) results from ThermoCalc Scheil module calculations. Dotted line defines crack susceptible composition range from Fig. 4

fication temperature range increasing as the nominal concentration of Cu decreases. Second, no terminal Cu rich liquid is expected when Ni concentrations exceed 30%.

Two characteristic types of solidification sequences were revealed by the Scheil calculations for the Fe–Ni–Cu system. The first sequence involved two face centered cubic (FCC) phases, one primary, the second terminal. This is shown in Fig. 11; a plot of fraction solid versus temperature for the Fe–10.0Ni–24.0Cu deposit. In this case, two distinct phases form, which is consistent with the microstructure for this sample in Fig. 8, where the terminal (intercellular) phase is Cu and the primary cells are a Fe–Ni–Cu solid solution γ phase. The second type of solidification sequence resulted in only one FCC phase upon solidification. A representative figure that shows this behavior can be seen in Fig. 12, which is a fraction solid versus

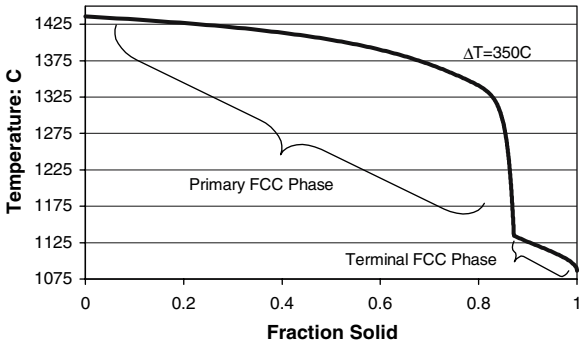

Fig. 11 Calculated fraction solid versus temperature with solidified phases for Fe–10.0Ni–24.0Cu. Solidifies as two FCC phases, one primary and one terminal

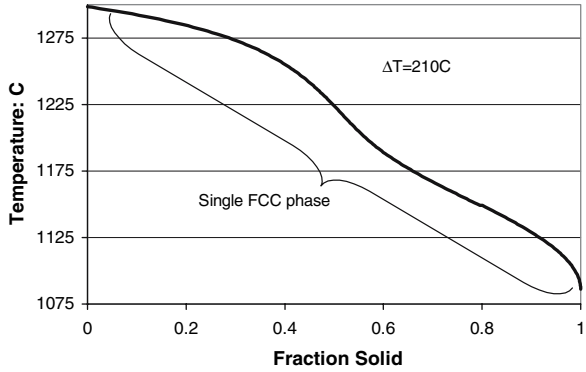

Fig. 12 Calculated fraction solid versus temperature with solidified phase designations for Fe–28.2Ni–57.8Cu. Solidifies as a single FCC phase

temperature plot for the Fe–28.2Ni–57.8Cu alloy. In this case, the microstructure does not show a distinct Cu rich phase, as shown in Fig. 9.

To ensure that the predicted trends for the Fe–Ni–Cu system are accurate, the calculations must be validated by experimental results. The first means of validation is comparing the predicted terminal Cu rich liquid and that measured in experimentally produced deposits. This comparison can only be made for deposits that exhibited a terminal Cu rich phase; i.e. for deposits with Ni concentration less than approximately 30 wt%. In Fig. 7 the predicted amount of terminal liquid can be compared with the experimental results. Increasing Ni content is expected to increase the solid solubility of Cu in the Fe–Ni matrix [9], thereby reducing the amount of Cu rich second phase, which is the case as shown in Fig. 7. However, it should be noted that in this particular case the Scheil calculation does not predict the greatest amount of terminal Cu rich phase. This is due to the retrograde solubility of Cu as observed in the Fe–Cu diagram. Scheil conditions will result in the greatest amount of terminal liquid only if the liquidus and solidus lines are monotonically decreasing, which is not the case in the Fe–Cu system. Under Scheil conditions of the Fe–Cu system, the solid that forms near the nose of the solidus will remain relatively rich in Cu, even though solid that forms at lower temperatures dissolves progressively less Cu. By comparison, under equilibrium conditions, all of the solid forming at the lower temperatures will have reduced Cu concentration, resulting in more segregation to the liquid. Thus, in this particular system with retrograde solubility, the solid actually dissolves more Cu in the Scheil condition than the equilibrium condition, resulting in a relatively lower amount of terminal Cu rich phase. It is expected that the retrograde solubility for Cu is present not only in the

Fe–Cu binary, but also in the Fe rich corner of the Fe–Ni–Cu ternary as these data suggest. The experimentally measured and Scheil calculated values show reasonable agreement, giving support to the Scheil simulations.

Comparing the predicted composition of each phase as a function of fraction solid formed was the second means of validation. Figure 13a is a scanning electron microscope (SEM) image taken of a cell in the Fe–10.0Ni–24.0Cu sample. EPMA data was taken across this cell. The white dots, which are most likely carbon contamination, were caused by the electron beam and serve as a useful guide to the location of the point measurements. The white intercellular region in the SEM image is Cu rich, as shown by the EPMA data presented in Fig. 13b. Figure 13b presents the EPMA data taken across the cell in Fig. 13a along with predicted composition of the solid as a function of fraction solid. The portion of the EPMA line scan is plotted as a function of normalized distance from the cell core to the cell boundary. An EPMA trace that goes across the center of a cell is equivalent to two traces made from the cell core to the intercellular region (e.g. Fig. 13a). This experimental data is compared to the Scheil calculations where the cell core is taken as $f_S = 0$ and the interdendritic region, where the Cu concentration peaks, is taken as $f_S = 1$. Figure 13c displays the same data as Fig. 13b but with a different y-axis scale, which better shows concentrations of Ni and Cu in the primary solid. In a similar fashion, EPMA line scans were made across secondary dendrite arms (Fig. 14) for the Fe–28.2Ni–57.8Cu alloy, which is expected to have only one solid phase with continu-

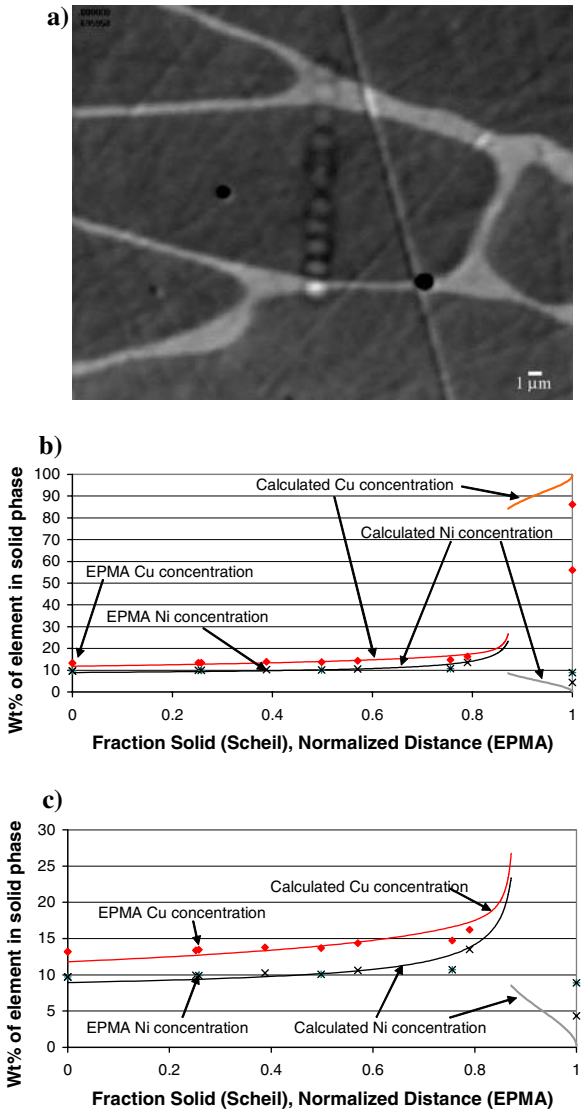

Fig. 13 (**a**) SEM micrograph of EPMA line scan on Fe–10.0Ni–24.0Cu. White dots are beam damage and indicate where compositional data was collected. (**b**) and (**c**) EPMA data and Scheil calculated concentration as a function of fraction solid formed plotted from 0 wt% to 100 wt% Cu and 0–30 wt% Cu, respectively

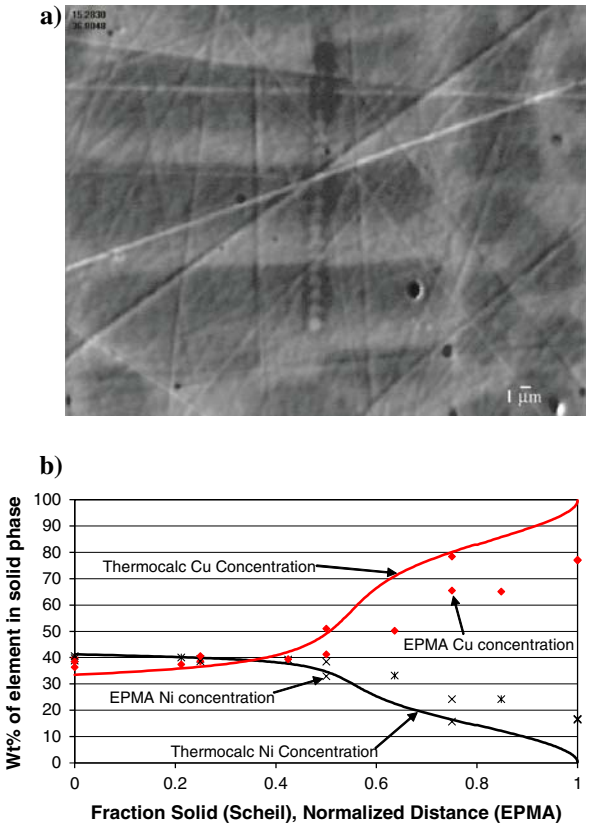

Fig. 14 (**a**) SEM micrograph of EPMA line scan on Fe–28.2Ni–57.8Cu. White dots are beam damage and indicate where compositional data was collected. (**b**) EPMA data and Thermo-Calc predicted concentration as a function of fraction solid formed

ously varying concentration. These EPMA traces were taken across the largest secondary arms observed, which indicates they are sectioned at or very near the mid-plane.

The agreement between measured and calculated phase fractions and solute profiles is reasonable. Differences between the calculated and experimentally measured concentrations may be the result of shifts in the phase boundary lines due to the effect of trace elements that were not included in the calculation. Additionally, the EPMAs ability to accurately measure the Cu rich intercellular concentrations in Fig. 13 is limited by the X-ray excitation volume of a 15 kV beam, which is on the order of 1 μm; approximately the same size as the intercellular region. Given the capabilities of the EPMA, and the potential effect of trace elements, reasonable agreement exists between the calculated and measured compositions.

Microstructural development provides an additional means to verify the ThermoCalc model results. There is a marked difference in the as-solidified microstructures of Figs. 8 and 9, as a distinct Cu rich second phase is absent in the latter. A second phase is not anticipated to form in an isomorphous system, such as Ni–Cu, even under Scheil solidification conditions. In an isomorphous phase diagram, the liquidus and solidus lines converge at the end of solidification, as can be seen for Ni–Cu in Fig. 1. Physically, this means that all the solute in the liquid is absorbed by the single solid phase, thereby preventing the formation of a terminal liquid.

Unlike a binary system, the liquidus and solidus lines in a ternary system follow a three-dimensional surface. The direction of their motion is dictated by the partition coefficients of each element and the diffusivity of solute elements in the primary phase. As such, isopleths constructed from a ternary phase diagram are of little use since they are constrained to two dimensions. ThermoCalc provides the capability to obtain compositional data for phases as a function of temperature. This data is derived from the composition of solid and liquid at any given temperature along the solidus and liquidus surfaces. This compositional data, obtained from the solidification pathway in three dimensions, can then be plotted in two dimensions (temperature and composition) to form ''pseudo'' solidus and liquidus lines. The shape of the liquidus and solidus lines can provide insight on phase formation during solidification.

Figures 15 and 16 display pseudo liquidus and solidus lines for Fe–10.0Ni–24.0Cu and Fe–28.2Ni–57.8Cu alloys, respectively. The shape of the Cu pseudo liquidus and solidus in the former alloy is of somewhat similar shape to the binary Fe–Cu liquidus and solidus lines. The composition of these lines drastically changes at 1135 °C upon the formation of the second phase, which is Cu rich. In the Fe–28.2Ni–57.8Cu the shape of the Ni and Cu liquidus and solidus lines are of similar shape to those observed in an isomporphous diagram. The solidus and liquidus lines merge at the end of solidification, thereby precluding the formation of a terminal phase.

Cracking susceptibility

The solidification temperature range and terminal liquid data presented in Fig. 10 can be used to explain the solidification cracking of Fig. 4. A large solidification temperature range exists with Fe–Cu, Ni–Cu and Fe–Ni–Cu alloys. Additionally, significant amounts of terminal Cu rich liquid are formed for Ni concentrations less than 30 wt%. The combination of these two factors controls the cracking susceptibility of Fe–Ni–Cu alloys with less than 30 wt% Ni. Cracking susceptibility increases with both solidification temperature range,

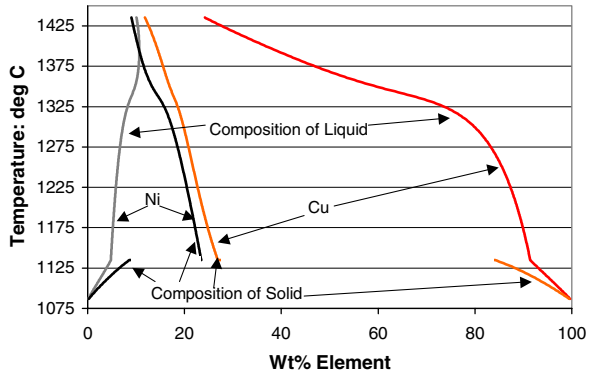

Fig. 15 Pseudo solidus and liquidus lines for Ni and Cu in Fe–10.0Ni–24.0Cu alloy

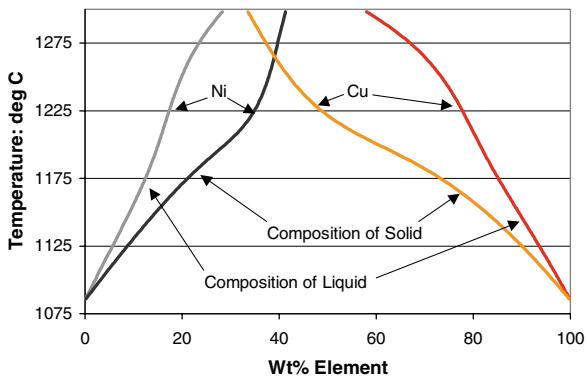

Fig. 16 Pseudo solidus and liquidus lines for Ni and Cu in Fe–28.2Ni–57.8Cu

and the amount of terminal liquid until there is sufficient terminal liquid to backfill any cracks that may develop.

Even when there is no terminal Cu (Ni concentrations > 30 wt%), due to solidification as a single phase, there remains a large solidification temperature range of 250 °C or greater in ternary alloys that crack. However, binary Ni–Cu alloys with similar solidification temperature range and absence of terminal liquid do not crack. This indicates that factors other than solidification temperature range and the amount of terminal liquid play a significant role in the solidification cracking susceptibility of Fe–Ni–Cu alloys.

It has been shown that the distribution of liquid in the solid + liquid "mushy zone" can also play a factor in solidification cracking susceptibility [29]. Thermo-Calc is able to calculate how the fraction liquid varies with temperature as an alloy solidifies. For temperature in the mushy zone to be converted to distance the thermal conductivity of the substrate must be known. The exact thermal conductivity of these substrates in many of the deposits is unknown since they are multi layered. This precludes converting liquidus temperature of an alloy to distance in the mushy zone. However, examining how fraction liquid varies with temperature for alloys that have similar solidification temperature ranges can provide a representative understanding of mushy zone behavior in alloys with similar solidification temperature range. In Fig. 17, fraction liquid as a function of temperature is plotted for three pairs of alloys that have the same solidification temperature range and no terminal liquid. The Fe–Ni–Cu alloy compositions fall within the compositional cracking range displayed in Fig. 4, whereas the Ni–Cu alloys were crack free.

Two important trends are observed. First, for any given temperature in the mushy zone, there is more liquid present in the Fe–Ni–Cu alloys. This will promote the formation of continuous liquid films along which solidification cracking may occur. Second, the amount of liquid at any temperature increases as Cu concentration is increased at the expense of Fe, while Ni concentration remains constant, but there is still insufficient liquid to back fill any cracks that may form even when the Cu concentration is 50 wt%.

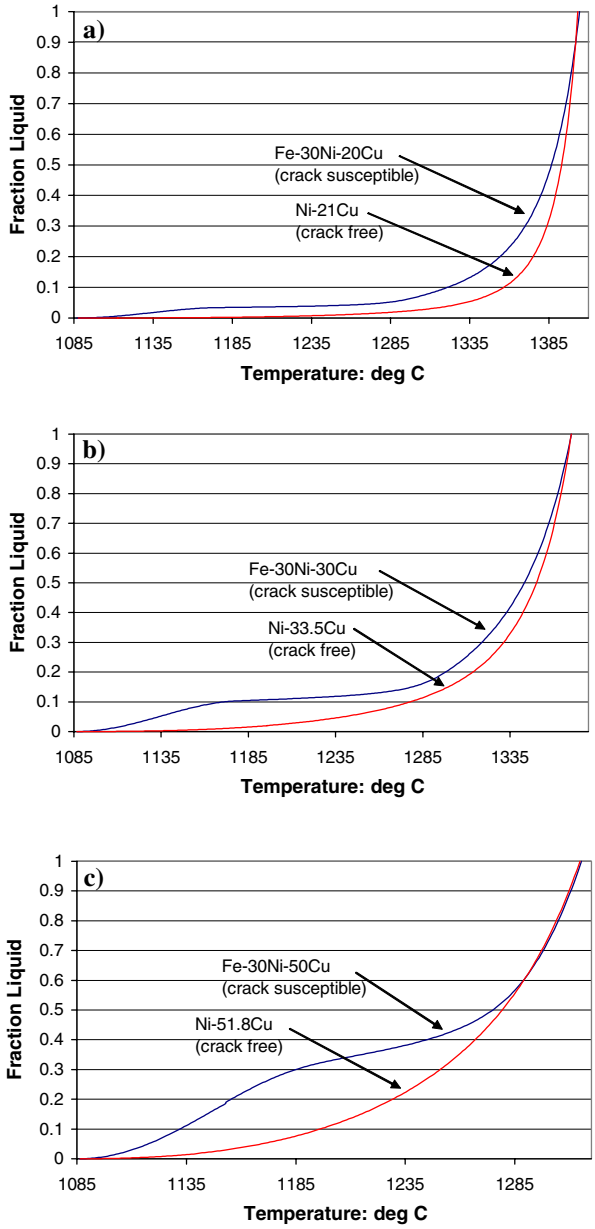

Fig. 17 Calculated variation of fraction liquid with temperature in the mushy zone for three alloys that do not form terminal liquid. (**a**) Fe–30Ni–20Cu and Ni–21Cu. Both alloys have a solidification temperature range of 314 °C. (**b**) for Fe–30Ni–30Cu and Ni–33.5Cu. Both alloys have a solidification temperature range of 280 °C. (**c**) for Fe–30Ni–50Cu and Ni–51.8Cu. Both alloys have a solidification temperature range of 206 °C

Conclusion

To determine the compositional cracking susceptibility of the Fe–Ni–Cu system, a wide range of Fe–Ni–Cu deposits was fabricated by GTAW with a cold wire feed. EPMA measurements were carried out to determine the composition of the deposits. Solidification cracking was observed when Cu was deposited onto Fe–Ni with Ni concentration of up to 75 wt% Ni.

The ThermoCalc Scheil model was validated for the Fe–Ni–Cu system by comparison with experimental results, which showed good agreement with the Scheil calculations. ThermoCalc Scheil calculations predicted a solidification temperature range of more than 150 °C

for nearly the entire ternary under Scheil solidification behavior.

Additionally, alloys with less than approximately 30 wt% Ni solidified as two FCC phases, whereas alloys with more than 30 wt% Ni were found to solidify as a single FCC phase. The solidification temperature range and amount of terminal liquid, which are effected by alloy composition, along with the mushy zone behavior, explain the solidification cracking susceptibility in the Fe–Ni–Cu system.

To produce functionally graded deposit of Steel, Ni and Cu that are free of solidification cracks, the concentration of the Ni interlayer must be 100 wt%.

Acknowledgement The authors gratefully acknowledge support of this work by the National Science Foundation through a PECASE Award, Grant No. DMI 9983968, made through the Division of Manufacturing and Industrial Innovation of NSF.

References

1. Thermal conductivity: metallic elements and alloys, vol 1, ed., Touloukian YS, IFI/Plenum, New York, Washington, 1970
2. Carpenter Technology Alloy Data: No. 883 (AISI H-13) Tool Steel
3. Asnis EA, Prokhorenko VM, Shvindlerman LS (1965) Mechanism of cracking during the welding or depositing of copper on to steel. Weld Production 12(11):15
4. Vainterman AE, Osetnik AA (1968) The formation of cracks during the deposition of copper alloys on steel. Automated Weld 21(6):22
5. Cooper RB, Burns TH (1974) Metals Eng Quart 14(3):41
6. Dixon B (1974) Aust Welding J 26(4):23
7. Noecker II FF, DuPont JN (2002) Functionally graded copper–steel using laser engineered net shaping process. Solid Freeform Fabrication Symposium Proceedings, pp 231–238
8. Noecker II FF, DuPont JN (2005) Microstructural development and solidification cracking susceptibility of Cu deposits on steel: Part 1. J Mater Sci 2005
9. Salter WJM (1966) J Iron Steel Institute, London 204(5):473
10. Rao KP, Periyasamy A (1992) Praktische Metallographie 29(11):564
11. Nippes EF, Ball DJ (1982) Copper-contamination cracking: cracking mechanism and crack inhibitors. Welding Research, Miami, FL, USA, pp 75–81
12. Borisenko MM et al (1975) Effect of copper and nickel on some properties of weld metal. Svarochnoe Proizvodstvo 1975(12):29
13. Swartzendruber LJ (1990) In: Thaddeus HO, Massalski B, Subramanian PR, Kacprzak L (eds) Binary alloy phase diagrams. ASM International, Materials Park, Ohio, pp 1408–1410
14. Scheil E (1942) Zeitschrift fur Metallkunde 34/35:70
15. Gupta KP (1990) The Cu–Fe–Ni (copper–iron–nickel) system, in phase diagrams of ternary nickel alloys. Indian Institute of Metals, Calcutta, pp 290–315
16. Goldstein JI et al (1992) Quantitative x-ray analysis: theory and practice, in scanning electron microscopy and x-ray microanalysis. Plenum, New York and London, pp 417–523
17. Brody HD, Flemings MC (1966) Trans Metallur Soc AIME 236(5):615
18. Brooks, JA (1990) Weld microsegregation: modeling and segregation effects on weld performance. Weldability Mater., Proc. Mater. Weldability Symp., pp 41–47
19. DuPont JN (1999) Microstructural development and solidification cracking susceptibility of a stabilized stainless steel. Welding Research (Miami), 1999(July), pp 253S–263S
20. DuPont JN (1996) Metallur Mater Trans A: Phys Metallur Mater Sci 27A(11):3612
21. Clyne TW, Wolf M, Kurz W (1982) Metallur Trans B: Process Metallur 13B(2):259
22. Rosenthal D (1946) Trans A.S.M.E 68:849
23. DuPont, JN, Marder AR (1996) In: Trends in Welding Research, Proceedings of the International Conference, 4th, Gatlinburg, Tenn., June 5–8, 1995, pp 449–454
24. Diffusion in metals, in Smithells metals reference book, Brook G, Brandes EA (eds) 1992, Butterworth-Heinemann, Oxford, Boston, Section 13
25. Sundman B (1990) Anales de Fisica, Serie B: Aplicaciones, Metodos e Instrumentos 86(2, Espec):69
26. Sundman B, Jansson B, Andersson JO (1985) CALPHAD: Computer Coupling of Phase Diagrams and Thermochemistry 9(2):153–190
27. Andersson JO et al (2002) CALPHAD: Computer Coupling of Phase Diagrams and Thermochemistry 26(2):273–312
28. Jansson B et al (1993) The Thermo-Calc database system. Comput. Software Chem. Extr. Metall., Proc. Int. Symp. 2nd, pp 57–71
29. DuPont JN, Robino CV, Marder AR (1999) Sci Technol Weld Join 4(1):1–14